

Split-Post Microwave Displacement Transducer with Quadratic Readout

Sonali Parashar*, Jeremy F. Bourhill, Maxim Goryachev, Michael E. Tobar^{1,*}

¹*Quantum Technologies and Dark Matter Labs, Department of Physics, University of Western Australia, 35 Stirling Highway, Crawley, WA 6009, Australia.*

(Dated: February 10, 2026)

We investigate a microwave cavity-based displacement readout employing a split-post geometry for measuring the motion of a dielectric membrane. The cavity response to membrane displacement is predominantly quadratic when the membrane is positioned at the centre of the posts. We characterise this behaviour by driving the membrane piezo electrically at both central and off-centre positions and calibrating the displacement using an independent interferometric measurement. The calibration reveals a linear coupling between the membrane displacement and the applied drive voltage, while the microwave response follows the static displacement dependence. When the membrane is driven at the centre, the system exhibits the highest displacement-to-voltage sensitivity and the largest quadratic output. As the membrane is moved away from the centre, the response gradually transitions from quadratic to linear. There is a difference of 97 % in the quadratic coefficient from the central position and a difference of 92 % in the linear coefficient from the off-centre position. This controllable crossover between quadratic and linear coupling is a key requirement for sensors capable of resolving energy quantisation. It establishes this platform as a promising candidate for a microwave-mechanical quantum transducer.

I. INTRODUCTION

The interaction between mechanical elements and microwave cavities is central to the field of cavity optomechanics, offering powerful means to manipulate photons via their coupling to phonons [1]. Such hybrid systems operate across a wide temperature range, from room temperature (RT) down to cryogenic conditions (4 K and milli-Kelvin), and have enabled the development of ultra-sensitive displacement transducers [2]. A variety of architectures have been employed to detect mechanical motion in MW-based systems. Common approaches use 3D lumped-element (LCR) microwave resonators incorporating a mechanical element [2], or qubit-based dispersive readouts where the microwave resonator couples to a superconducting qubit, which acts as the readout for mechanical motion [3–7]. For low-noise operation at milli-Kelvin temperatures, junction-based parametric amplifiers have been developed to enhance signal-to-noise ratios [8–11], to achieve the standard quantum limit, and similar techniques extend to readouts based on SQUID-based amplifiers [12, 13].

Mechanical resonators come in diverse forms, including bulk acoustic wave (BAW) [14–18] and surface acoustic wave (SAW) devices [19], thin membranes [20–23], and even lower-dimensional photonic structures [24, 25]. These can be integrated on-chip as micro-/nanomechanical hybrid resonators coupled to microwave or optical photons [26–28]. The electromagnetic cavities

themselves may be realised as lumped-element re-entrant modes [29–34], whispering gallery modes [35–38], or travelling-wave structures [9–11], including transmission line geometry [11]. Crucially, the opto-mechanical coupling between the microwave cavity mode and the mechanical displacement typically produces a linear coupling; however, higher-order dependencies of the microwave frequency on displacement can be engineered [39–43]. When cooled close to its motional ground state [13, 44], the mechanical mode enters the quantum regime [45], where its transitions obey Fermi’s golden rule [46]. Achieving ground-state cooling allows operation beyond the thermal noise floor [22, 47], and with sufficiently high cooperativity, a quadratic readout can effectively realise a multi-level quantum system [39–42, 48]. Such systems exhibit phenomena including strong opto-mechanical coupling [32], parametric amplification [23, 49], ground-state cooling, and squeezing [28] and can store quantum information in entangled states [39, 48]. Macroscopic mechanical elements are powerful platforms for probing the classical–quantum boundary [32, 50] and for sensing low-frequency signals, as their effective mass scales inversely with frequency. This makes them well suited to the kHz–MHz range, with applications to high-frequency gravitational-wave detection [51–55], resonant-mass gravitational antennas [56, 57], and dark-matter searches in the MHz–GHz band [34, 58], as well as precision tests of Lorentz symmetry [49, 50, 59] and the quantum nature of gravity [46, 60–64].

In this work, we present a split-post re-entrant microwave resonator engineered to realise a *quadratic* displacement readout. Re-entrant and microwave cavities have previously served as highly sensitive *linear* transducers [12, 29, 32], where the first-order frequency shift with displacement dominates the response. Here, the geometry and operating point are chosen to cancel the first-order sensitivity ($df/dx = 0$) at a symmetry (bias) point,

* sonali.parashar@research.uwa.edu.au
michael.tobar@uwa.edu.au

while enhancing the second-order term ($d^2 f/dx^2 \neq 0$), yielding a *purely quadratic* response. This capability enables direct access to displacement-squared observables, facilitates back-action-evasive measurements of mechanical energy, and opens up nonlinear opto-mechanical regimes inaccessible to conventional linear readouts. Re-entrant cavities additionally offer strong parametric coupling [12, 65, 66], broadband tunability, and compatibility with ultra-low-noise detection, resulting in a versatile platform for quantum-limited sensing.

II. THEORETICAL FRAMEWORK

The system under investigation comprises a mechanical membrane resonator, enclosed within a microwave cavity that incorporates a split-post geometry. This symmetry is analogous to that of a membrane-in-the-middle opto-mechanical system, where the membrane interacts with the electromagnetic field confined between two re-entrant posts. A schematic representation of the cavity topology is shown in Fig. 1. In the ideal symmetric configuration, the membrane is positioned exactly at the cavity's mid-plane, the Fig. 1(a), equidistant from the opposing posts. The parameter d_i denotes the separation between the two posts. In this configuration, we anticipate a purely quadratic dependence of the cavity frequency on the motion of the membrane due to the system's symmetry: the frequency shift caused by a positive displacement x of the dielectric membrane inside the cavity's \vec{E} field will be identical to that caused by a negative displacement, giving rise to pure quadratic coupling to the cavity membrane. Whereas, when the membrane is positioned off-centre as shown in Fig. 1(b), the system symmetry is broken, with positive and negative displacements being no longer symmetric in the cavity field basis, which can be interpreted as sampling an off-center region of the expected quadratic displacement (x_2 in Fig. 1(c)), which can be approximated as a linear relationship for small displacements. As the post-separation increases (i.e. d_2 compared to d_1), the expected quadratic relationship between membrane displacement and cavity frequency is weakened, as would be expected as $d \rightarrow \infty$.

If the cavity frequency ω_c is expressed as a Taylor expansion around the symmetry point $x = 0$, we can write:

$$\omega_c(x) = \omega_c(0) + G_1 x + \frac{1}{2} G_2 x^2 + \dots \quad (1)$$

Here ω_0 is the unperturbed cavity resonant frequency with the membrane located at $x = 0$, δx is the displacement of the mechanical resonator, and $G_n = \partial^n \omega_c / \partial x^n|_{x=0}$. When the membrane's starting position is the cavity centre (symmetry line) we know that $\omega_c(x) = \omega_c(-x)$ and can therefore state that:

$$G_1 = \left. \frac{\partial \omega_c}{\partial x} \right|_{x=0}, \quad G_2 \neq 0, \quad (2)$$

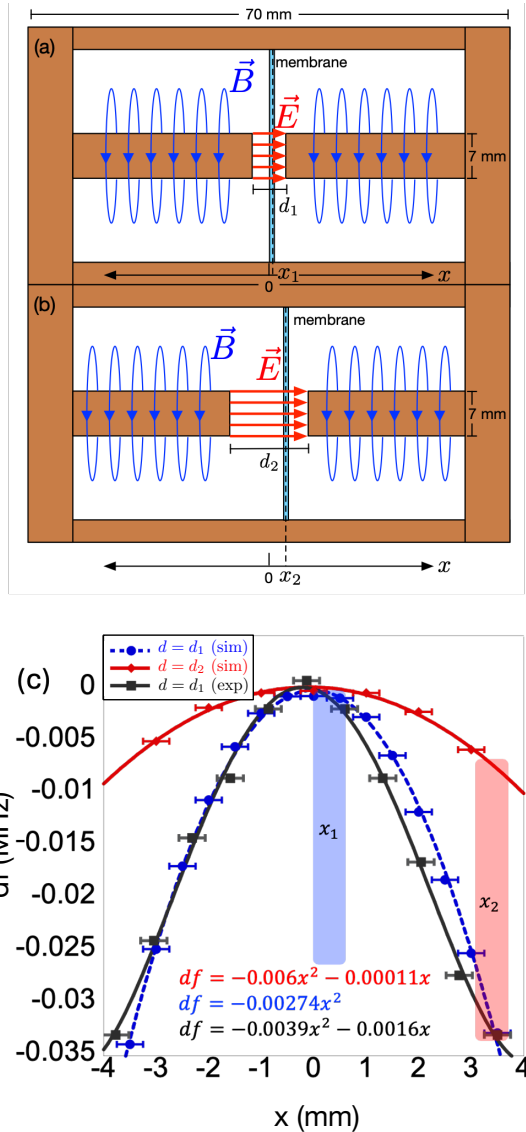


FIG. 1. (a,b) Schematics of the split-post re-entrant resonator with an acoustic membrane. The cavity electric field is axial and localised between the post end faces, while the magnetic field \vec{B} circulates around each post. The mechanical modes of the central membrane modulate the microwave field. The post-separation is d_1 in (a) and d_2 in (b). The membrane positions are x_1 (symmetric, a) and x_2 (asymmetric, b). (c) Shows the change in microwave resonant frequency versus membrane position from FEM simulations and experiment. Experimentally, a VNA tracks the resonant frequency by monitoring S_{21} as the membrane is moved between the posts.

implying an even function and quadratic coupling to the lowest order. In the off-centre position, we insert $x =$

$x_0 + \delta x$:

$$\begin{aligned}\omega_c(x_0 + \delta x) &\approx \omega_c(0) + \frac{1}{2}G_2(x_0 + \delta x)^2, \\ &= \omega_c(0) + \frac{1}{2}G_2x_0^2 + G_2x_0\delta x + \frac{1}{2}G_2(\delta x)^2, \\ &= \omega_c(x_0) + (G_2x_0)\delta x + \frac{1}{2}G_2(\delta x)^2.\end{aligned}\quad (3)$$

We note that a linear dependence on displacement emerges as a result of sampling the function's curvature at the asymmetric offset position. The dependence of the microwave frequency on the membrane's displacement results in a standard opto-mechanical Hamiltonian description [1, 39–42]:

$$\hat{H} = \hat{H}_{MW} + \hat{H}_{mech} + \hat{H}_{int}, \quad (4a)$$

$$\hat{H}_{MW} = \hbar\omega_c(\hat{a}^\dagger\hat{a}), \quad (4b)$$

$$\hat{H}_{mech} = \hbar\omega_m(\hat{b}^\dagger\hat{b}), \quad (4c)$$

$$\hat{H}_{int} = \hbar(g_1(\hat{b} + \hat{b}^\dagger) + g_2(\hat{b} + \hat{b}^\dagger)^2)(\hat{a}^\dagger\hat{a}). \quad (4d)$$

Here, we see that the system Hamiltonian is the sum of three sub-system Hamiltonians: a photon term representing the microwave cavity mode, \hat{H}_{MW} , a phonon term corresponding to the mechanical membrane mode, \hat{H}_{mech} , and an interaction term describing their mutual coupling, \hat{H}_{int} . In the above equations, \hat{a} (\hat{a}^\dagger) represent the annihilation (creation) operators for microwave photons in the resonant cavity, whilst \hat{b} (\hat{b}^\dagger) represent the annihilation (creation) operators for mechanical phonons in the membrane drum mode, which are related to the displacement operator by $\hat{x} = x_{zpf}(\hat{b} + \hat{b}^\dagger)$, where x_{zpf} is the zero-point fluctuation displacement of the mechanical system (displacement created by single phonon occupancy). The coupling terms $g_1 = G_2x_0x_{zpf}$ and $g_2 = \frac{1}{2}G_2x_{zpf}^2$ represent the linear and quadratic opto-mechanical coupling rates. Thus, we can see in the $x_0 = 0$ symmetric case, the linear term g_1 vanishes and the interaction Hamiltonian is purely quadratic.

If the cavity is strongly and coherently driven with the membrane in the symmetric case ($g_1 = 0$), we can state that $a = \alpha + \delta a$, $|\alpha|^2 = \bar{n}_{cav}$, where α is the complex intra cavity field amplitude and \bar{n}_{cav} is the mean intra cavity photon number. In this approximation, we can therefore write the interaction part of the Hamiltonian as:

$$\hat{H}_{int} = \hbar g_2(|\alpha|^2 + \alpha^*\delta a + \alpha\delta a^\dagger)(\hat{b} + \hat{b}^\dagger)^2, \quad (5)$$

Here α^* is the complex conjugate of the field amplitude. Expanding the $(\hat{b} + \hat{b}^\dagger)^2$ term gives:

$$\hat{H}_{int} = \hbar g_2(|\alpha|^2 + \alpha^*\delta a + \alpha\delta a^\dagger)(1 + 2\hat{b}^\dagger\hat{b} + \hat{b}^2 + \hat{b}^{\dagger 2}), \quad (6)$$

which when combined with \hat{H}_{mech} and taking the rotating wave approximation (RWA), which allows the $\hat{b}^{\dagger 2}$ and \hat{b}^2 terms to be dropped, allows us to redefine the mechanical Hamiltonian as:

$$\hat{H}'_{mech} \approx \hbar(\omega_m + 2g_2|\alpha|^2)\hat{b}^\dagger\hat{b}. \quad (7)$$

This is equivalent to the optical spring effect but originating from a quadratic coupling: the cavity photon population stiffens (or softens) the mechanical oscillator, hence changing its resonant frequency.

Ignoring the small signal terms in eq. (6) we can now rewrite the system Hamiltonian as $\hat{H} = \hat{H}'_{mech} + \hat{H}_{MW} + \hat{H}'_{int}$, where

$$\hat{H}'_{int} = 2\hbar g_2(\alpha^*\delta a + \alpha\delta a^\dagger)\hat{b}^\dagger\hat{b}, \quad (8)$$

which implies that microwave cavity fluctuations δa are linearly coupled to the phonon number operator $\hat{b}^\dagger\hat{b}$. This permits a quantum non-demolition measurement of the phonon-number state (and hence mechanical resonator energy) via the cavity field phase, and is the primary reason a quadratic readout is desirable.

III. EXPERIMENTAL SETUP

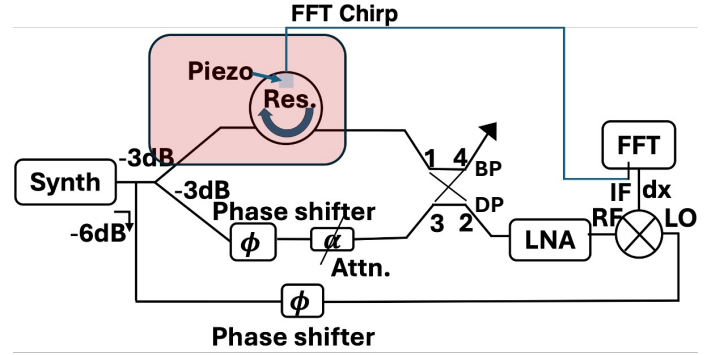


FIG. 2. Experimental setup used to observe the mechanical membrane mode inside the split-post microwave resonator. The interferometric measurement techniques ensure that the signal at the DP is minimised, enabling maximum suppression of the unwanted signals. A spectrum analyser (FFT) is used to excite the PZT actuator and read the output of the interferometer. $\partial V_{mix}/\partial \omega_c$ is the interferometer sensitivity and is maximum when the DP have zero signal.

To observe the opto-mechanical interaction, we drive the membrane into mechanical motion using a piezoelectric transducer (PZT) mounted on the body of the microwave resonator. The interaction between the membrane displacement x and the piezo driving voltage, V_{PZT} , applied at the mechanical frequency, is expected to be linear. This relationship will be dictated by the mechanical mode-specific transfer function of the PZT displacement to membrane displacement, $S(\omega)$ multiplied by the conversion of PZT drive voltage into actuator displacement ($R(\omega)$):

$$x(\omega) = S(\omega)R(\omega)V = T(\omega)V_{PZT}, \quad (9)$$

where $T(\omega)$ is the combined transfer function which will evaluate out to a constant real value for a given drive

frequency ω . This displacement will then produce a frequency shift of the microwave cavity through the optomechanical mechanism described by (3). In the symmetric setup of the Fig. 1(a) we therefore anticipate a purely quadratic dependence of cavity frequency on applied PZT voltage.

The dynamic response of the opto-mechanical system is measured by an interferometric microwave setup as shown in Fig. 2. In essence, the interferometer functions to produce an output voltage proportional to the difference in phase between its two arms, one of which contains the opto-mechanical device, whose phase will be modulated by the frequency shift induced by membrane displacement (homodyne detection scheme). We characterize the interferometer's sensitivity to the microwave resonator frequency shift by the term $\frac{\partial V_{mix}}{\partial \omega_c}$, which is a product of the strength of microwave coupling to the microwave resonant mode, the microwave Q -factor, incident power, and the mixer conversion efficiency, among other parameters. The sensitivity can be measured by driving the microwave resonator in the interferometer with a frequency-modulated source (mimicking the effect of membrane oscillations) and measuring the mixer output (∂V_{mix}) at the modulation frequency for a given amplitude of frequency modulation ($\partial \omega_c$).

An interferometric readout technique ensures that the entire setup is sensitive to even the smallest phase changes by suppressing the large amplitude carrier signal, enabling the use of a low noise amplifier (LNA) [67, 68]. The interferometric measurement setup is driven by a microwave frequency synthesiser that drives both the interferometer and the local oscillator (LO) port of the readout mixer. The signal is divided across the two arms of the interferometer: the test arm, which contains the microwave resonator, and the balance arm, which contains a phase shifter and attenuator. These two arms are then recombined through a hybrid coupler, with the balance arm components carefully tuned to ensure carrier suppression of the difference signal at the dark port (DP) output of the coupler. That is to say, the large amplitude signal at the microwave resonance frequency is suppressed via destructive interference at the interferometer output, enabling the use of a low noise amplifier (LNA), which would otherwise be saturated, to greatly enhance the amplitude of fluctuations of the carrier (modulation sidebands) caused by modulations in the test arm. The LNA output is then mixed down with the LO signal, which is phase shifted to ensure mixer IF voltage is proportional to the phase difference between the LO and RF signals, and then sent to a spectrum analyser or fast Fourier transform (FFT) machine. This allows the detection of phase changes due to variations in the microwave cavity frequency, corresponding to the linear response of the mechanical resonator's membrane mode [69]. The setup shown in Fig. (2) shows the interferometric readout setup.

The above-discussed settings for the interferometric setup ensure that the voltage-to-frequency sensitivity of

the microwave readout is maximised once the interferometer is perfectly balanced. The interferometric setup was operated with a sensitivity of $\partial V_{mix}/\partial \omega_c = 0.6 - 0.7$ mV/kHz at various membrane positions x inside the microwave cavity. With a change in the gap size between the split post resonator, the loaded quality factor of the resonator changes, resulting in a slight change in the sensitivity of the interferometric readout. The readout for the membrane mode excitation by the piezoelectric transducer is observed by measuring the effective phase shift (or frequency change) of the microwave signal and is read from the IF port of the mixer. The microwave cavity, along with the PZT, is housed inside a vacuum chamber, with the vacuum level maintained at $1 \cdot 10^{-5}$ mbar at RT. Whilst the FFT measures the mixer output, connected to input channel 1, the PZT is simultaneously excited using a chirp source from the FFT, followed by a low-pass filter.

With this sensitivity parameter known, one can now interpret the amplitude of the interferometer's mixer output when the membrane is driven by the PZT actuator as frequency shifts of the microwave resonator. If the value of G_2 and membrane initial position x_0 are both known, or equivalently, an approximation of $\partial \omega_c/\partial x$ can be determined for the membrane's initial position (i.e. by statically changing the position of the membrane and reading out microwave frequency, as will be demonstrated later), the inferred frequency shift from the mixer output voltage can then be used to determine the membrane's displacement via the following relationship:

$$\partial V_{mix} = \frac{\partial \omega_c}{\partial x} \frac{\partial V_{mix}}{\partial \omega_c} \partial x = \frac{\partial \omega_c}{\partial x} \frac{\partial V_{mix}}{\partial \omega_c} T(\omega) \partial V_{PZT}, \quad (10)$$

which can then be related to the applied actuator voltage, V_{PZT} , as shown. Thus, by varying V_{PZT} and monitoring V_{mix} , we can obtain information regarding the nature of $\partial \omega_c/\partial x$ given the linear relationship between ∂V_{PZT} and ∂x . In fact, this linear relationship (eq.(9)) can also be experimentally determined by examining the dependence of inferred displacement (from V_{mix} and eq.10) and applied actuator voltage V_{PZT} , as will be shown. The microwave cavity was specifically engineered to interrogate a sapphire membrane with a diameter of 50 mm and a thickness of 0.5 mm. The cavity geometry was optimised using COMSOL MULTIPHYSICS simulations to support a re-entrant mode in the frequency range of 5-6 GHz. The overall cavity length was set to 70 mm to achieve the desired frequency while maintaining strong mode confinement and field localisation between the posts. In the optimised design Fig. 1(a), the membrane was positioned symmetrically between the two re-entrant posts, with a nominal separation of $d_1 = 1.5$ mm. A second, asymmetric membrane position was also investigated, which required a larger post-separation to ensure asymmetric positioning Fig. 1(b). In this configuration, $d_2 = 10$ mm and the crystal was positioned at $x_0 = +3.5$ mm.

The microwave cavity was characterised using a VNA.

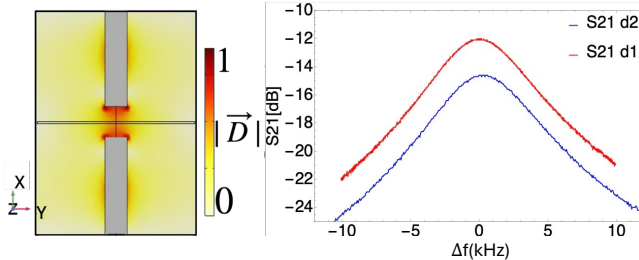


FIG. 3. The microwave resonator: (a) cross-section of the microwave cavity with absolute electric field displacement of the microwave resonator represented by \vec{D} (b) The microwave mode characterisation by transmission parameter S_{21} for the d_1 and d_2 positions in the Fig. 1 in terms of the mode frequency offset during the change in the post .

The Fig. 3 shows the microwave cavity displacement response in COMSOL simulations and the characterisation of the microwave cavity by measuring S_{21} . The microwave S_{21} parameter, where the gap between the posts is ~ 4 mm, is recorded. The frequency of the microwave resonance with the membrane position, as in the Fig. 19a) measured to be $\omega_c/2\pi = 5.3206$ GHz, with a loaded quality factor of $Q_l = 1530$, however the membrane position, as in the Fig. 1(b) measured to be at the offset of 115 kHz from $\omega_c/2\pi = 5.3206$ GHz with a loaded quality factor of $Q_l = 1130$. An input power P_{in} of 0.01 W is injected into the microwave resonator for the experiments conducted at RT.

The mechanical properties of the sapphire membrane were modelled using COMSOL. This allowed the determination of membrane mode resonant frequencies. The membrane external boundary was clamped, and the eigenfrequencies, modal masses, and participation factors of the drum modes were evaluated. The fundamental membrane drum mode resonant frequency was simulated to be 4.169 kHz. Tuning the PZT actuator drive across this frequency and observing the mixer output from the interferometer reveals the existence of this resonant mode and its ability to couple to the microwave resonator. The Fig. (4) represents (a) the fundamental drum mode simulated absolute displacement denoted by $|dx|$, and (b) the mixer output voltage V_{mix} reading the fundamental drum mode.

IV. RESULTS AND DISCUSSION

We investigate the nature of $\partial\omega_c/\partial x$ in two ways: firstly by recording the microwave resonant frequency as the static position x_0 of the crystal is changed for two different post-separations, $d_1 = 1.5$ mm and $d_2 = 10$ mm. Secondly, the dynamic response of the microwave resonator is measured using the interferometric setup of the Fig. 2 as the membrane is driven via the PZT actuator, for the membrane positioned symmetrically

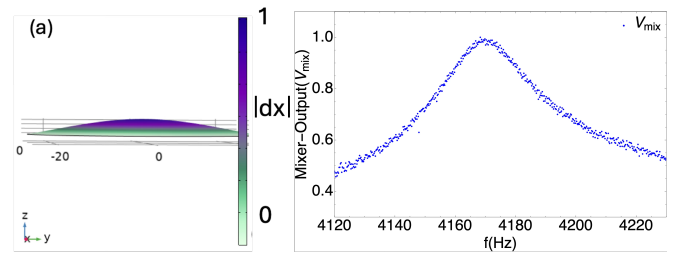


FIG. 4. The mechanical resonance of the sapphire membrane: (a) simulation of the fundamental drum mode, showing the crystal's absolute displacement. (b) The measured frequency response of this resonance at $\omega_m/2\pi = 4.169$ kHz. The mode is excited using a PZT drive and read via the mixer output of the interferometer.

($x_0 \approx 0$) with post-separation $d_1 = 1.5$ mm, as well as an asymmetric position $x_0 = 3.5$ mm with post-separation $d_2 = 10$ mm. The static measurements of the microwave cavity resonance frequency were experimentally monitored using a vector network analyser (VNA). The experiment was conducted by tracking the peak of the microwave cavity resonance, measured via transmission S_{21} . By manually changing the membrane position x_0 , which is mounted on a movable platform inside the microwave resonator, the static response of the microwave cavity is measured. These results confirmed a *quadratic dependence* of cavity frequency on crystal displacement, consistent with the symmetric split-post geometry that suppresses the first-order (linear) coupling term. These experimental results are shown by the (black trace in the Fig. 1(c), where each data point corresponds to the resonant frequency of the split-post cavity with a different position of the membrane inside, with post separation d_1 . COMSOL simulation of the cavity eigenfrequency as the sapphire membrane position x_0 is changed between the posts also verifies this result (blue trace in the Fig. 1(c)). Similar results but with a smaller G_2 value are observed with post separation d_2 (red trace in the Fig. 1(c)).

The dynamic response of the resonator is measured by driving the membrane with a PZT and measuring the changes in the microwave cavity phase via microwave interferometry. Experiments were conducted to drive the membrane in both the central and off-central positions of the membrane.

The interferometric output was recorded while driving the fundamental membrane mode with the PZT, giving it a linear displacement. As discussed in the eq.(10) and experimentally shown in Fig. 4. This gives rise to the change in the microwave resonance frequency. Which leads to a phase shift corresponding to the drum mode resonance frequency. Hence, by recording the change in the peak of the drum mode resonance frequency from the output port of the mixer with changing PZT voltage, a response for ∂V_{mix} versus ∂V_{PZT} is obtained. A chirp signal is applied to the PZT with a voltage that is varied from 10mV to 1000mV. The chirp frequency was

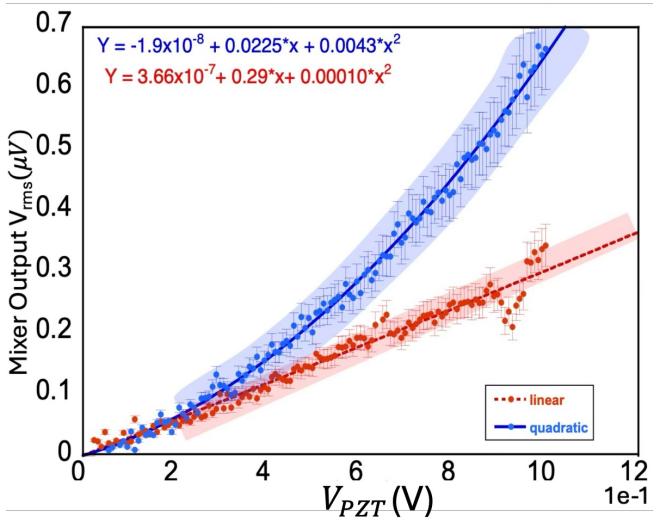


FIG. 5. Mixer output voltage (V_{mix}) as a function of applied voltage to the piezoelectric drive (V_{PZT}), when the membrane is driven with a chirp signal with ω_m as the central frequency. Blue data is for the membrane positioned at the central, symmetric position, whilst red shows the off-centre position.

centred around ω_m . The peak of the mixer output trace (V_{mix}) was plotted against the applied excitation voltage to the piezoelectric crystal (V_{PZT}). The blue trace in Fig. 5 shows the mixer output when driven at the central position, whilst the red trace shows the off-central response.

These results confirm a quadratic response in the central case, whilst an overwhelmingly linear response is observed in the asymmetric case, as predicted by eq. (3). This reveals the capability to generate either linear or quadratic opto-mechanical coupling within the one system, dependent purely on the membrane's initial position, due to the symmetrical nature of the microwave resonance. The displacement of the membrane x with applied PZT drive (V_{PZT}) from the experimental data is also evaluated to confirm the theoretical response and is shown in Fig. 6. These results confirm that the displacement is linear for both cases. Here blue trace represents Fig. 1(a), and the red trace represents Fig. 1(b). This corresponds to the response of the membrane displacement outlined in the eqn. (10).

The interferometric setup was calibrated for the different membrane displacement x_i versus applied PZT voltage. This response shows the behaviour of the PZT, and is shown in the Fig. 5 and is explained by the eq.(10). The experimental value of the $T(\omega)$ is evaluated to be 1 nm/mV by measuring the slope of this measured data set. Ideally, a mixer should have no DC component, but due to mixer imbalance, it produces a DC output, leading to a non-zero output voltage with no PZT voltage applied. This is called the DC offset. Removing this offset does not change the fit parameter. The results shown in the Fig. 5 show the interferometric readout output with quadratic and linear fits to the data points as the

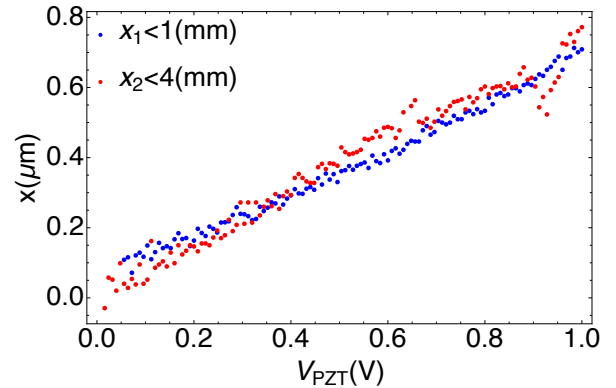


FIG. 6. Inferred crystal displacement x as a function of applied PZT voltage V_{PZT} . microwave cavity frequency shift is derived from readout output V_{mix} and readout sensitivity $\partial V_{mix} / \partial \omega_c$, which can then be converted into crystal displacement from the static measurement of $\partial \omega_c / \partial x \propto G_2$ attained by tracking microwave resonance frequency as crystal position is changed. The linear slope of both datasets (blue for symmetric and red for asymmetric membrane positions) represents $T(\omega)$: the transfer function from applied PZT voltage V_{PZT} to crystal displacement, which we expect to be very similar for both crystal positions.

PZT voltage is varied and the Mixer-Output voltage is recorded, with the DC offset removed.

Therefore, driving the membrane at different locations within the split-post resonator results in an output response that is either quadratic or linear, depending on the position of the membrane inside the microwave cavity readout and confirms the static response of the microwave resonator. Comparing the results shown in eq. (1) with those demonstrated in the Fig. 5, their behaviour and second-order coupling rates can be evaluated. The value of G_2 comes out to be around $5.37 * 10^{-16}$ Hz that is deduced using eq. (9) and the curve fitting parameters in the Fig. 5.

V. CONCLUSION

It was demonstrated that the split-post microwave cavity readout exhibited parametric quadratic behaviour due to the intrinsic symmetry of the microwave resonance. When the sapphire membrane was positioned at the centre or off-centre within the microwave resonator, the output response appeared quadratic or linear, respectively. This parametric readout system had the potential to be developed into a transducer capable of measuring energy when operated in its ground state. This work could be scaled to a single-graviton detection scheme, in which kilogram-scale detectors were impedance-matched to gram-scale detectors to measure energy deposited by a gravitational wave at kHz frequencies and thereby probe energy quantization. Such an approach, when enabled by ground-state cooling of the resonator, could yield promis-

ing results, particularly for phonon counting by building strongly coupled detectors capable of measuring energy [46, 64]. Our analysis further showed that the split-post resonator had a higher aspect ratio and greater field overlap in the region of the mechanical modes [32] than a

single-post resonator [31, 32], resulting in a higher output coupling rate. By incorporating these features of split-post resonators, we were able to read out a non-piezoelectric membrane and characterise its response, contributing to the development of a quadratic transducer.

[1] Markus Aspelmeyer, Tobias J Kippenberg, and Florian Marquardt. Cavity optomechanics. *Reviews of Modern Physics*, 86(4):1391, 2014.

[2] Shabir Barzanjeh, André Xuereb, Simon Gröblacher, Mauro Paternostro, Cindy A Regal, and Eva M Weig. Optomechanics for quantum technologies. *Nature Physics*, 18(1):15–24, 2022.

[3] VI Shnyrkov, AP Shapovalov, V Yu Lyakhno, AO Dumanik, AA Kalenyuk, and Pascal Febvre. An rf squid readout for a flux qubit-based microwave single photon counter. *Superconductor Science and Technology*, 36(3):035005, 2023.

[4] Mingyun Yuan, Vibhor Singh, Yaroslav M Blanter, and Gary A Steele. Large cooperativity and microkelvin cooling with a three-dimensional optomechanical cavity. *Nature communications*, 6(1):8491, 2015.

[5] Raphaël Lescanne, Samuel Deléglise, Emanuele Albertinale, Ulysse Réglade, Thibault Capelle, Edouard Ivanov, Thibaut Jacqmin, Zaki Lehtas, and Emmanuel Flurin. Irreversible qubit-photon coupling for the detection of itinerant microwave photons. *Physical Review X*, 10(2):021038, 2020.

[6] A Romanenko, R Harnik, A Grassellino, R Pilipenko, Y Pischalnikov, Z Liu, OS Melnychuk, B Giaccone, O Pronitchev, T Khabiboulline, et al. Search for dark photons with superconducting radio frequency cavities. *Physical review letters*, 130(26):261801, 2023.

[7] OA Ilinskaya, AI Ryzhov, and SN Shevchenko. Flux qubit based detector of microwave photons. *Physical Review B*, 110(15):155414, 2024.

[8] JY Mutus, TC White, Evan Jeffrey, Daniel Sank, Rami Barends, Joerg Bochmann, Yu Chen, Zijun Chen, Ben Chiaro, Andrew Dunsworth, et al. Design and characterization of a lumped element single-ended superconducting microwave parametric amplifier with on-chip flux bias line. *Applied Physics Letters*, 103(12), 2013.

[9] F Lecocq, L Ranzani, GA Peterson, K Cicak, RW Simmonds, JD Teufel, and J Aumentado. Nonreciprocal microwave signal processing with a field-programmable josephson amplifier. *Physical Review Applied*, 7(2):024028, 2017.

[10] Chris Macklin, K O’brien, D Hover, ME Schwartz, V Bolkhovsky, X Zhang, WD Oliver, and I Siddiqi. A near-quantum-limited josephson traveling-wave parametric amplifier. *Science*, 350(6258):307–310, 2015.

[11] Farzad Faramarzi, Sasha Sypkens, Ryan Stephenson, Byeong H Eom, Henry Leduc, Saptarshi Chaudhuri, and Peter Day. A near quantum limited sub-ghz tin kinetic inductance traveling wave parametric amplifier operating in a frequency translating mode. *arXiv preprint arXiv:2406.00530*, 2024.

[12] Michael E Tobar. Characterizing multi-mode resonant-mass gravitational wave detectors. *Journal of Physics D: Applied Physics*, 28(8):1729, 1995.

[13] Chris Whittle, Evan D Hall, Sheila Dwyer, Nergis Mavalvala, Vivishek Sudhir, Robert Abbott, A Ananyeva, C Austin, L Barsotti, Joseph Betzwieser, et al. Approaching the motional ground state of a 10-kg object. *Science*, 372(6548):1333–1336, 2021.

[14] Maxim Goryachev, Daniel L Creedon, Eugene N Ivanov, Serge Galliou, Roger Bourquin, and Michael E Tobar. Extremely low-loss acoustic phonons in a quartz bulk acoustic wave resonator at millikelvin temperature. *Applied Physics Letters*, 100(24), 2012.

[15] Serge Galliou, Maxim Goryachev, Roger Bourquin, Philippe Abbé, Jean Pierre Aubry, and Michael E Tobar. Extremely low loss phonon-trapping cryogenic acoustic cavities for future physical experiments. *Scientific reports*, 3(1):2132, 2013.

[16] Yiwen Chu, Prashanta Kharel, William H. Renninger, Luke D. Burkhardt, Luigi Frunzio, Peter T. Rakich, and Robert J. Schoelkopf. Quantum acoustics with superconducting qubits. *Science*, 358(6360):199–202, 2017.

[17] Yu Yang, Igor Kladarić, Maxwell Drimmer, Uwe von Lüpke, Daan Lenterman, Joost Bus, Stefano Marti, Matteo Fadel, and Yiwen Chu. A mechanical qubit. *Science*, 386(6723):783–788, 2024.

[18] Hilel Hagai Diamandi, Yizhi Luo, David Mason, Tevfik Bulent Kanmaz, Sayan Ghosh, Margaret Pavlovich, Taekwan Yoon, Ryan Behunin, Shruti Puri, Jack G. E. Harris, and Peter T. Rakich. Optomechanical control of long-lived bulk acoustic phonons in the quantum regime. *Nature Physics*, 21(9):1482–1488, 2025.

[19] Kevin Joseph Satzinger, YP Zhong, H-S Chang, Gregory A Peairs, Audrey Bienfait, Ming-Han Chou, AY Cleland, Christopher R Conner, Étienne Dumur, Joel Grebel, et al. Quantum control of surface acoustic-wave phonons. *Nature*, 563(7733):661–665, 2018.

[20] NC Carvalho, J Bourhill, ME Tobar, and OD Aguiar. Sensitivity characterisation of a parametric transducer for gravitational wave detection through optical spring effect. *Classical and Quantum Gravity*, 34(17):175001, 2017.

[21] CR Locke, ME Tobar, and EN Ivanov. Properties of a monolithic sapphire parametric transducer: prospects of measuring the standard quantum limit. *Classical and Quantum Gravity*, 19(7):1877, 2002.

[22] CR Locke and ME Tobar. Measurement of the strain-induced coefficient of permittivity of sapphire using whispering gallery modes excited in a high-q acoustic sapphire oscillator. *Measurement Science and Technology*, 15(10):2145, 2004.

[23] Sumit Kumar, Matthew Kenworthy, Henry Ginn, and Xavier Rojas. Optomechanically induced transparency/absorption in a 3D microwave cavity architecture at ambient temperature. *arXiv preprint arXiv:2406.00530*, 2024.

arXiv:2402.10935, 2024.

[24] Yanhao Tang and Kin Fai Mak. 2d materials for silicon photonics. *Nature nanotechnology*, 12(12):1121–1122, 2017.

[25] Arafa H Aly, Fatma A Sayed, and Hussein A Elsayed. Defect mode tunability based on the electro-optical characteristics of the one-dimensional graphene photonic crystals. *Applied optics*, 59(16):4796–4805, 2020.

[26] Shlomi Kotler, Raymond W Simmonds, Dietrich Leibfried, and David J Wineland. Hybrid quantum systems with trapped charged particles. *Physical Review A*, 95(2):022327, 2017.

[27] AA Clerk, KW Lehnert, P Bertet, JR Petta, and Y Nakamura. Hybrid quantum systems with circuit quantum electrodynamics. *Nature Physics*, 16(3):257–267, 2020.

[28] Igor Marinkovic, Maxwell Drimmer, Bas Hensen, and Simon Groblacher. Hybrid integration of silicon photonic devices on lithium niobate for optomechanical wavelength conversion. *Nano letters*, 21(1):529–535, 2021.

[29] Ben T McAllister, Yifan Shen, Graeme Flower, Stephen R Parker, and Michael E Tobar. Higher order reentrant post modes in cylindrical cavities. *Journal of Applied Physics*, 122(14), 2017.

[30] NC Carvalho, J Bourhill, M Goryachev, S Galliou, and ME Tobar. Piezo-optomechanical coupling of a 3D microwave resonator to a bulk acoustic wave crystalline resonator. *Applied Physics Letters*, 115(21), 2019.

[31] Jeremy Bourhill, Natalia do Carmo Carvalho, Maxim Goryachev, Serge Galliou, and Michael E Tobar. Generation of coherent phonons via a cavity enhanced photonic lambda scheme. *Applied Physics Letters*, 117(16), 2020.

[32] S Parashar, WM Campbell, J Bourhill, E Ivanov, M Goryachev, and ME Tobar. Upconversion of phonon modes into microwave photons in a lithium niobate bulk acoustic wave resonator coupled to a microwave cavity. *APL Photonics*, 9(11), 2024.

[33] Natalia C Carvalho, Yaohui Fan, Jean-Michel Le Floch, and Michael Edmund Tobar. Piezoelectric voltage coupled reentrant cavity resonator. *Review of Scientific Instruments*, 85(10), 2014.

[34] M. Hirschel, V. Vadakkumbatt, N. P. Baker, F. M. Schweizer, J. C. Sankey, S. Singh, and J. P. Davis. Superfluid helium ultralight dark matter detector. *Phys. Rev. D*, 109:095011, May 2024.

[35] Michael Edmund Tobar, John Gideon Hartnett, and James David Anstie. Proposal for a new michelson-morley experiment using a single whispering spherical mode resonator. *Physics Letters A*, 300(1):33–39, 2002.

[36] Joaquim José Barroso, Pedro José de Castro, Odylio Denys de Aguiar, and LA Carneiro. Reentrant cavities as electromechanical transducers. *Review of scientific instruments*, 75(4):1000–1005, 2004.

[37] Albert Schliesser and Tobias J Kippenberg. Cavity optomechanics with whispering-gallery mode optical microresonators. In *Advances In Atomic, Molecular, and Optical Physics*, volume 58, pages 207–323. Elsevier, 2010.

[38] Maxim Goryachev, Warrick G Farr, Daniel L Creedon, and Michael E Tobar. Controlling a whispering-gallery-doublet-mode avoided frequency crossing: Strong coupling between photon bosonic and spin degrees of freedom. *Physical Review A*, 89(1):013810, 2014.

[39] AM Jayich, JC Sankey, BM Zwickl, C Yang, JD Thompson, SM Girvin, AA Clerk, F Marquardt, and JGE Harris. Dispersive optomechanics: a membrane inside a cavity. *New Journal of Physics*, 10(9):095008, 2008.

[40] JD Thompson, BM Zwickl, AM Jayich, Florian Marquardt, SM Girvin, and JGE Harris. Strong dispersive coupling of a high-finesse cavity to a micromechanical membrane. *Nature*, 452(7183):72–75, 2008.

[41] Roel Burgwal, Javier del Pino, and Ewold Verhagen. Comparing nonlinear optomechanical coupling in membrane-in-the-middle and single-cavity systems. *New Journal of Physics*, 22(11):113006, 2020.

[42] Igor Brandão, Bruno Suassuna, Bruno Melo, and Thiago Guerreiro. Entanglement dynamics in dispersive optomechanics: Nonclassicality and revival. *Physical Review Research*, 2(4):043421, 2020.

[43] André Xuereb and Mauro Paternostro. Selectable linear or quadratic coupling in an optomechanical system. *Physical Review A—Atomic, Molecular, and Optical Physics*, 87(2):023830, 2013.

[44] James Schneeloch, Erin Sheridan, A Matthew Smith, Christopher C Tison, Daniel L Campbell, Matthew D LaHaye, Michael L Fanto, and Paul M Alsing. Principles for optimizing quantum transduction in piezo-optomechanical systems. *arXiv preprint arXiv:2312.04673*, 2023.

[45] Jun-Ya Yang, Dong-Yang Wang, Cheng-Hua Bai, Si-Yu Guan, Xiao-Yuan Gao, Ai-Dong Zhu, and Hong-Fu Wang. Ground-state cooling of mechanical oscillator via quadratic optomechanical coupling with two coupled optical cavities. *Optics express*, 27(16):22855–22867, 2019.

[46] Germain Tobar, Sreenath K Manikandan, Thomas Beitel, and Igor Pikovski. Detecting single gravitons with quantum sensing. *Nature Communications*, 15(1):7229, 2024.

[47] Peter R Saulson. Thermal noise in mechanical experiments. *Physical Review D*, 42(8):2437, 1990.

[48] Taofiq K Paraíso, Mahmoud Kalae, Leyun Zang, Hannes Pfeifer, Florian Marquardt, and Oskar Painter. Position-squared coupling in a tunable photonic crystal optomechanical cavity. *Physical Review X*, 5(4):041024, 2015.

[49] Paul L Stanwix, Michael E Tobar, Peter Wolf, Mohamad Susli, Clayton R Locke, Eugene N Ivanov, John Winterflood, and Frank Van Kann. Test of lorentz invariance in electrodynamics using rotating? format?; cryogenic sapphire microwave oscillators. *Physical review letters*, 95(4):040404, 2005.

[50] PA Bushev, J Bourhill, Maxim Goryachev, N Kukharchyk, E Ivanov, Serge Galliou, ME Tobar, and S Danilishin. Testing the generalized uncertainty principle with macroscopic mechanical oscillators and pendulums. *Physical Review D*, 100(6):066020, 2019.

[51] Maxim Goryachev and Michael E Tobar. Gravitational wave detection with high frequency phonon trapping acoustic cavities. *Physical Review D*, 90(10):102005, 2014.

[52] Nancy Aggarwal, Odylio D Aguiar, Andreas Bauswein, Giancarlo Cella, Sebastian Clesse, Adrian Michael Cruise, Valerie Domcke, Daniel G Figueroa, Andrew Geraci, Maxim Goryachev, et al. Challenges and opportunities of gravitational-wave searches at mhz to ghz frequencies. *Living reviews in relativity*, 24:1–74, 2021.

[53] Maxim Goryachev, William M Campbell, Ik Siong Heng, Serge Galliou, Eugene N Ivanov, and Michael E Tobar. Rare events detected with a bulk acoustic wave high frequency gravitational wave antenna. *Physical Review Let-*

ters, 127(7):071102, 2021.

[54] William M Campbell, Ben T McAllister, Maxim Goryachev, Eugene N Ivanov, and Michael E Tobar. Searching for scalar dark matter via coupling to fundamental constants with photonic, atomic, and mechanical oscillators. *Physical Review Letters*, 126(7):071301, 2021.

[55] William M Campbell, Maxim Goryachev, and Michael E Tobar. The multi-mode acoustic gravitational wave experiment: Mage. *Scientific Reports*, 13(1):10638, 2023.

[56] Geert Dick van Albada, J Flokstra, G Frossati, Edward PJ van den Heuvel, JW van Holten, ATAM de Waele, and PKA Witt de Huberts. Grail r&d proposal. 1997.

[57] David G Blair, Eugene N Ivanov, Michael E Tobar, PJ Turner, Frank Van Kann, and IS Heng. High sensitivity gravitational wave antenna with parametric transducer readout. *Physical Review Letters*, 74(11):1908, 1995.

[58] Asimina Arvanitaki, Savas Dimopoulos, and Ken Van Tilburg. Sound of dark matter: searching for light scalars with resonant-mass detectors. *Physical review letters*, 116(3):031102, 2016.

[59] Anthony Lo, Philipp Haslinger, Eli Mizrachi, Loïc Anderegg, Holger Müller, Michael Hohensee, Maxim Goryachev, and Michael E Tobar. Acoustic tests of Lorentz symmetry using quartz oscillators. *Physical Review X*, 6(1):011018, 2016.

[60] Thiago Guerreiro, Francesco Coradeschi, Antonia Micol Frassino, Jennifer Rittenhouse West, and Enrico Junior Schioppa. Quantum signatures in nonlinear gravitational waves. *Quantum*, 6:879, 2022.

[61] BD Cuthbertson, ME Tobar, EN Ivanov, and DG Blair. Parametric back-action effects in a high-Q cryogenic sapphire transducer. *Review of Scientific Instruments*, 67(7):2435–2442, 1996.

[62] JT Hsiang, HT Cho, and BL Hu. Graviton physics: a concise tutorial on the quantum field theory of gravitons. *Graviton Noise, and Gravitational Decoherence, Universe*, 10(306):2405–11790, 2024.

[63] Germain Tobar, Sreenath K Manikandan, Thomas Beitel, and Igor Pikovski. Detecting single gravitons with quantum sensing. *arXiv preprint arXiv:2308.15440*, 2023.

[64] Markus Aspelmeyer. When zeh meets feynman: How to avoid the appearance of a classical world in gravity experiments. In *From Quantum to Classical: Essays in Honour of H.-Dieter Zeh*, pages 85–95. Springer, 2022.

[65] Michael E Tobar, Clayton R Locke, Eugene N Ivanov, Ik Siong Heng, and David G Blair. Accurate calibration technique for a resonant-mass gravitational wave detector. *Review of Scientific Instruments*, 71(11):4282–4285, 2000.

[66] CR Locke, ME Tobar, EN Ivanov, and DG Blair. Parametric interaction of the electric and acoustic fields in a sapphire monocrystal transducer with a microwave readout. *Journal of applied physics*, 84(12):6523–6527, 1998.

[67] CA Regal, JD Teufel, and KW Lehnert. Measuring nanomechanical motion with a microwave cavity interferometer. *Nature Physics*, 4(7):555–560, 2008.

[68] Richard A Woode, Eugene N Ivanov, and Michael E Tobar. Application of the interferometric noise measurement technique for the study of intrinsic fluctuations in microwave isolators. *Measurement Science and Technology*, 9(9):1593, 1998.

[69] Doyle A Ellerbruch. Evaluation of a microwave phase measurement system. *J. Res. NBS*, 69:55–65, 1965.